ACS APPLIED MATERIALS & INTERFACES

Research Article

www.acsami.org

Probing Opto-Mechanical Stresses within Azobenzene-Containing Photosensitive Polymer Films by a Thin Metal Film Placed Above

Nataraja Sekhar Yadavalli,*[,†] Denis Korolkov,[‡] Jean-François Moulin,[§] Margarita Krutyeva,[∥] and Svetlana Santer[†]

[†]Department of Experimental Physics, Institute of Physics and Astronomy, University of Potsdam, 14476 Potsdam, Germany

[‡]Bruker AXS GmbH, Oestliche Rheinbrueckenstrasse 49, 76187 Karlsruhe, Germany

[§]Helmholtz Zentrum Geesthacht, Institut für Werkstoffforschung, Abteilung WPN, Instrument REFSANS, Lichtenbergstrasse 1, 85747 Garching FRM II, Germany

[∥]Jülich Centre for Neutron Science JCNS (JCNS-1) & Institute for Complex Systems (ICS-1), Forschungszentrum Jülich GmbH, 52425 Jülich, Germany

Supporting Information

ABSTRACT: Azo-modified photosensitive polymers offer the interesting possibility to reshape bulk polymers and thin films by UV-irradiation while being in the solid glassy state. The polymer undergoes considerable mass transport under irradiation with a light interference pattern resulting in the formation of surface relief grating (SRG). The forces inscribing this SRG pattern into a thin film are hard to assess experimentally directly. In the current study, we are proposing a method to probe opto-mechanical stresses within polymer films by characterizing the mechanical response of thin metal films (10 nm) deposited on the photosensitive polymer. During irradiation, the metal film not only deforms along with the SRG formation but ruptures in a regular and complex manner. The morphology of the cracks differs strongly depending on the electrical field distribution in the interference pattern, even when the magnitude and the kinetics of the strain are kept constant. This implies a complex local distribution of the opto-mechanical stress along the topography grating. In addition, the neutron reflectivity measurements of the metal/polymer interface indicate the penetration of a metal layer within the polymer, resulting in a formation of a bonding layer that confirms the transduction of light-induced stresses in the polymer layer to a metal film.

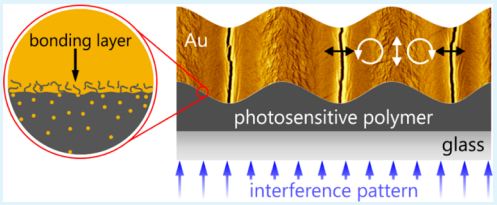

KEYWORDS: *surface relief grating, opto-mechanical stresses, bonding layer at the metal/polymer interface, rupturing of metal film, metal/multilayered graphene/polymer interfaces, azobenzene*

1. INTRODUCTION

Azobenzene-containing polymers belong to a class of functional materials exhibiting a strong coupling between an external radiation field and the mechanical response of the polymer film. These materials comprise two molecular components, one of which constitutes a polymer matrix and the other an ensemble of azobenzene (azo) moieties that are attached to the polymers as side chains. It is now well-established that the azobenzene molecules can undergo a reversible trans−cis photoisomerization process when excited with a polarized light beam, leading to a quasi-permanent molecular reorientation in a direction perpendicular to polarization of the incident light. As a result, the photosensitive film exhibits a strong topographical response upon irradiation with light.[1−4] During this process, the polymer film follows the distribution of intensity or polarization within the interference pattern and deforms, resulting in formation of surface relief grating (SRG).[5−8] The mass transport of polymer occurs in macroscopically regular and periodic fashion across the polymer surface.[9−12] This is very promising for applications in data storage, diffractive optical elements, micro- and nanofabrication of complex periodic structures for plasmonic studies, trapping of light in solar cells, and deformable electronics.[13−18]

From an academic point of view, the question about the physical origin of the SRG formation remains still open. What one could say with certainty is that the electric field induces a local, spatially varying alignment of azo molecules.[19−22] Most probably the mechanical response on the macroscale is a multiscale chain of physicochemical phenomena, including small scale motion of azo molecules due to the local change in their chemical potential upon isomerization, the collective alignment of azo molecules and their coupling to the polymer backbone that they are connected to, and finally the changing elastic properties of the polymer.[23−33]

Recently, we have solved experimentally a very important question: how does the local state of polarization of the impinging light interference pattern relate to the change in topography and the orientation of the azobenzene molecules. Here, a homemade setup combining an optical part and an

Received: March 27, 2014
Accepted: July 4, 2014
Published: July 4, 2014

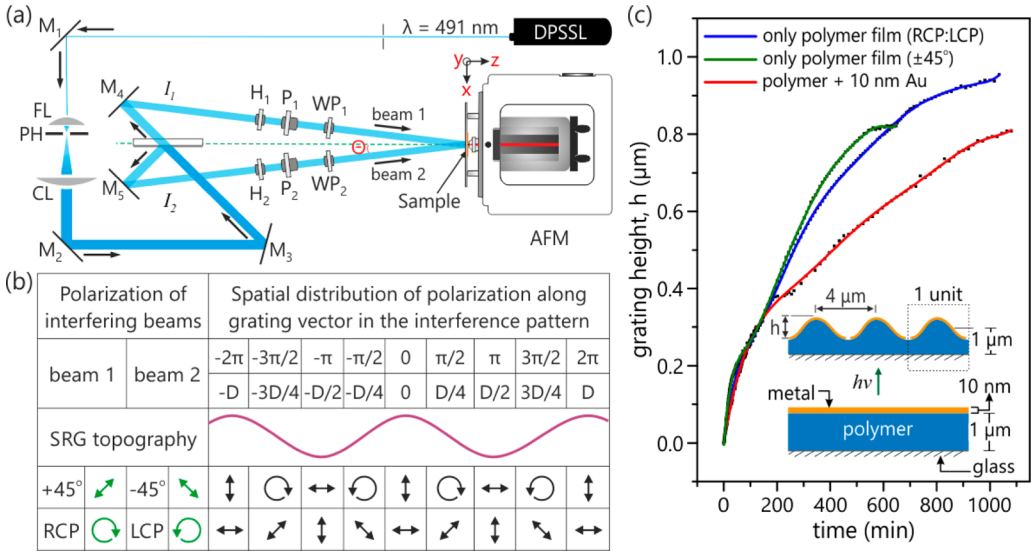

Figure 1. (a) Scheme of the homemade setup combining AFM and a Mach–Zehnder interferometer to inscribe SRG in photosensitive polymer and to record the grating growth kinetic: M_1, M_2, M_3, M_4, and M_5 are mirrors; BS is a beam splitter; H_1, H_2 are $\lambda/2$ plates; P_1, P_2 are polarizers; WP_1, WP_2 are $\lambda/2$ or $\lambda/4$ wave plates; I_1, I_2 are intensities of beams; and S is a computer-controlled shutter. (b) Spatial distributions of polarizations along the grating vector (x-axis) of the interference pattern used in the current investigation, for small interference angle (θ). The positions of the maxima and minima of the SRG are related to the electrical field distribution as shown by the red curve. (c) Grating growth kinetics for a polymer film using an RCP:LCP interference pattern (blue curve), for a polymer film using a ±45° pattern (green curve), and a polymer film with a 10 nm metal film deposited on top for both patterns (red curve). The inset scheme describes the grating profile parameters.

atomic force microscope has been established as described elsewhere.[2,3] Using this setup we have also reported on deformation of the metal layer placed above the photosensitive polymer film.[34] The fact that even with the strong constrain by the metal layer the polymer film still deforms indicates development of strong mechanical stress within the polymer films.

Ultrathin metal films (<10 nm) deposited on compliant polymer substrates are particularly interesting due to the fact that it is easy to achieve a continuously coated conductive metal film on polymer surfaces without a seeding layer[35,36] and with an added advantage of deformability compared to the deposition of metal film on conventional hard surfaces such as SiO_2. It is expected that physical deposition processes on polymer substrate leads to the penetration of metal islands near the polymer surface, creating a so-called bonding or sandwich layer, and the failure of thin electronics is mainly related to the quality of the bonding/sandwich layer at the interface due to delamination effects.[37] There are no clear reports on the nature of this bonding layer except a recent depth profiling study of 100 nm thick aluminum film deposited on polymer substrate analyzed via dynamic quadrupole secondary ion mass spectrometry with only partial success due to the lack of proper interface.[38]

In this study, we used neutron reflectometry and a metal/multilayered graphene/polymer interface system to probe the bonding layer at the ultrathin metal/polymer interface and its role in metal deformation. Moreover, we report on using the deformation of the metal layer for probing opto-mechanical stresses along the surface relief grating. To achieve a comprehensive understanding of the distribution and magnitude of surface and volume forces during mass redistribution in azobenzene-modified photosensitive polymer films, an appropriate and complete theory should be provided. We hope that our experimental observations could spark interesting theoretical work.

2. MATERIALS AND METHODS

2.1. Photosensitive Polymer. The azobenzene-containing photosensitive polymer PAZO (poly{1-[4-(3-carboxy-4-hydroxyphenylazo)-benzenesulfonamido]-1,2-ethanediyl, sodium salt}) is purchased from Sigma-Aldrich with molecular weight of $M_n = 1.4 \times 10^4$ g/mol (ca. 40 repeat units). The polymer solution is prepared by dissolving PAZO in a solvent mixture of 95% methoxyethanol and 5% ethylene glycol. To prepare a 1 μm thick polymer film, a polymer solution of 250 mg/mL concentration is spin-cast onto a glass substrate (thickness ~130 μm from Carl Roth GmbH) at 10 000 rpm during 1 min, followed by drying with nitrogen flow.

2.2. In-Situ AFM Connected Two Beam Interferometer. A simplified Mech-Zehnder interferometer (Figure 1a) is used to inscribe the surface relief gratings in PAZO films. As a source, a diode-pumped solid-state laser (Cobalt Calypso) operating in continuous wave and single longitudinal mode with high coherence at 491 nm wavelength is used. The polarization state of the output beam from laser source is in the vertical linear state. The beam is spatially expanded with a focusing lens (FL), passed through a pinhole (PH), and collimated with a collimating lens (CL). The uniform central part of the collimated Gaussian beam profile (5 mm diameter) is used further to generate the interference pattern. The beam is allowed to pass through a 50:50 (T:R) nonpolarizing beam splitter (BS) and split into two beams of equal intensities by the amplitude division principle.

The polarization state of each beam can be controlled with a set of retarders ($\lambda/2$ and/or $\lambda/4$ plates) and polarizers. The polarizers (P_1 and P_2) are used to make sure that the two beams after splitting at the beam splitter (BS) have only a vertically linear polarization state without other polarization noise. The half-wave plates H_1 and H_2 are positioned before the polarizers as shown in Figure 1a, for achieving equal intensities ($I_1 \sim I_2$) in both beams after passing through the polarizers based upon "Malus's law" ($I = I_{max} \cos^2\varphi$). To achieve a circularly polarized beam, it is well-known that any series combination of an appropriately oriented linear polarizer and a quarter-wave plate together perform as a circular polarizer. In our optical setup, quarter-wave plates (WP_1 and WP_2) are used for both beams with fast axes oriented orthogonal 45° to each other and to the incoming vertical linearly polarized beams to achieve right- and left-circularly polarized beams. To achieve a ±45° interference pattern, $\lambda/2$ plates are used

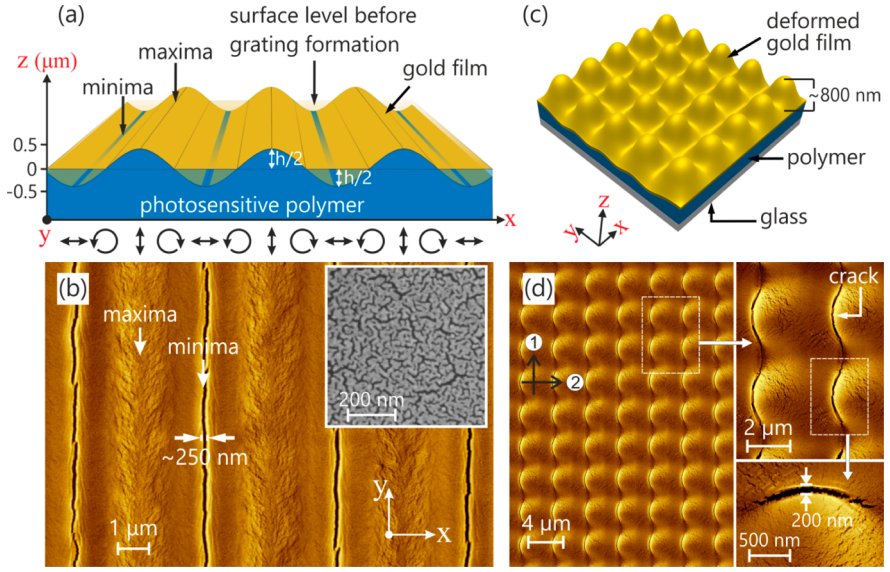

Figure 2. (a) Scheme of deformed metal film on polymer surface during SRG formation. (b) SEM micrograph of the periodically ruptured gold film on a polymer during SRG formation. The inset shows a high-resolution SEM image of the metal film consisting of a well-packed metal network. (c) Scheme of the sample shown as SEM micrographs in part d. The topography was formed by subsequent cross-irradiation with ±45° interference pattern.

instead of $\lambda/4$ plates. These orthogonal polarized beams [±45° or right circular polarized:left circular polarized (RCP:LCP)] are then aligned to interfere at the surface of a polymer sample such that simultaneous in-situ measurements of the grating formation with the AFM setup can be carried out. The irradiation of sample is achieved from the glass side (back side). The periodicity D of the optical interference pattern can be adjusted by controlling the angle 2θ between interfering beams as $D = \lambda/(2 \sin \theta)$, where λ is the wavelength of the laser source. All in-situ AFM measurements are performed using tapping-mode AFM (PicoScan, Agilent) with 1 Hz scan speed. The growth kinetics of SRG are obtained by programming the AFM scan cycle to maintain periodic up and down scanning during in situ measurements. With this setting, topography variations running upward and downward in the AFM images represent the topography changes across the whole polymer surface with time.

2.3. Neutron Reflectivity Measurements. The neutron reflectivity curves were obtained at the time-of-flight reflectometer REFSANS operated at the MLZ in Garching, Germany. The instrument was operated with an incident wavelength spectrum ranging from 2 to 10 Å with a $\Delta\lambda/\lambda$ resolution of 3%. The opening of the beam defining slits were selected as to keep the total $\Delta Q/Q = 6\%$. Using three consecutive overlapping measurements at incident angles 0.3°, 0.6° and 1.4°, the reflectivity was measured over the q range extending to 0.2 $Å^{-1}$.

3. RESULTS AND DISCUSSION

3.1. In-Situ AFM-Assisted Analysis of SRG Growth Kinetics. The kinetic of polymer surface deformation with and without a metal film on top during irradiation is recorded by a homemade setup combining an atomic force microscope (AFM) and Mach−Zehnder interferometer (Figure 1a). The two orthogonal polarized laser beams are aligned to interfere at the polymer sample positioned with the AFM for in-situ measurements of the topography change. In this study we apply two different polarization combinations of the interfering beams: +45°:−45° or ±45° and RCP:LCP. The distribution of the electrical field vector in the resultant polarization interference pattern at the point of interference along grating vector (x-axis) for both combinations is presented in Figure 1b. Using our experimental setup, we are able to measure a change in the grating height, i.e., the difference between the grating maxima to the grating minima, during irradiation as a function of time (Figure 1c). The periodicity of polymer grating is chosen to be 4 μm for all experiments, since at this value one gets the maximum achieved grating height of 970 ± 50 nm after 12 h of irradiation.

By taking the arc length $\{s = \int_0^{\pi}[1 + A_o^2\,(4\pi^2/\Lambda^2)(\cos(2\pi x/\Lambda))^2]^{1/2}\,dx\}$ of the deformed PAZO surface (sinusoidal profile), we estimated a maximum change in surface area, i.e., strain, of 14% during grating formation. Additionally, using the protocol introduced in our previous publications,[2,3] we were able to assign the positions of the maxima and minima of the topography to the distribution of the electrical field vector within the interference pattern (see the sinusoidal curve in Figure 1b).

3.2. Periodic Rupturing of Ultrathin Metal Films on Photosensitive Polymer. Ultrathin gold films of 100 ± 10 Å are deposited on a photosensitive polymer film via the physical vapor deposition process with an evaporation rate of 0.25 Å/s. The high-resolution scanning electron microscopy (SEM) migrograph of the metal film is shown in the inset of Figure 2b. The film consists of closely packed interconnected metal islands and possesses good conductivity with a resistance of 180 ± 20 Ω compared to the polymer film of infinite resistance. The conductivity of deposited metal film proves the good continuity of deposited metal films on the polymer surface.

The polymer film constrained by a 100 Å thick metal film still deforms during irradiation with an interference pattern; however, the maximum achievable grating height decreases to 780 ± 40 nm (red curve in Figure 1c). This deformation results in a 10.5% increase in surface area of the metal layer, i.e., strain. During deformation the metal layer ruptures periodically (Figure 2d), forming cracks of ~200 nm in width along the grating minima through out the irradiated region. The cracks start to appear only after several minutes of irradiation, when the grating height increases to more than half of the maximally attainable height (see Supporting Information, Figure S1). For instance, if the irradiation proceeds 200 min (see red curve in

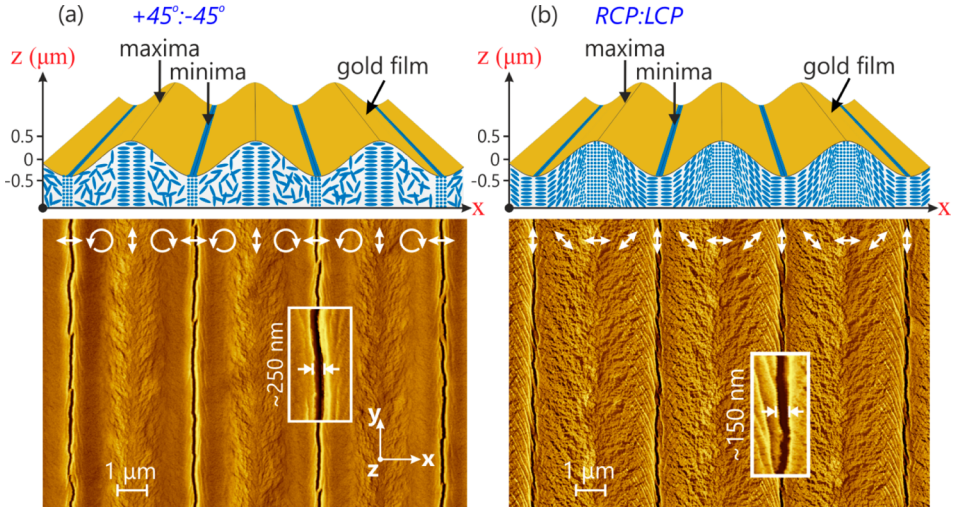

Figure 3. SEM micrographs of the metal layers deformed on the polymer film during inscription of the surface relief grating using two different polarization states of the interference pattern: (a) ±45° and (b) RCP:LCP. The distribution of the electrical vector relative to the topography variation is depicted by white arrows. For both cases, the schematical representation of azobenzene (depicted as blue ellipses) orientation in the polymer film after irradiation is shown above the SEM micrographs.

Figure 1c), the metal layer with inscribed SRG topography stays intact. Since in the azobenzene-containing photosensitive polymer films, opto-mechanical stress can be induced in repeated irradiation stages, we performed cross-irradiation in the subsequent step with the ±45° interference pattern by turning the sample 90° to the direction of the first irradiation. In the second step, irradiation was conducted up to a grating height of 800 nm. Again the metal film was ruptured at the topography minima, where uniform cracks of 200 nm in width appear (Figure 2d).

When the SRG is inscribed by an interference pattern of a different polarization state, for instance RCP:LCP, the metal layer is again ruptured at the topography minima (Figure 3b). However, at the same change in the height and periodicity of the surface grating, i.e., the same induced strain, the morphology of the deformed metal layer differs significantly.

Thus, when comparing the metal layer deformed by irradiation with ±45° (Figure 3a) and RCP:LCP (Figure 3b), one immediately recognizes that in the first case the metal between the wide cracks is almost undamaged with only subnanoscopic riffles at the topography maxima. In the case of RCP:LCP deformed metal, at the slopes of the SRG there are densely spread cracks progressing from grating minima toward maxima at an angle of 65° with respect to the grating vector. Additionally, metal wrinkles at the topography minima are detected (see for instance the enlargement in Figure 3b). SEM images of cracks spread across larger scan area are included in the Supporting Information (Figure S2). From this observation one can conclude that at the same applied strain and kinetics of the deformation (compare curves in Figure 1c) the local distribution of the strength and direction of the opto-mechanical load should be different for different polarization states of the interference patterns.

The periodic crack formation phenomenon presented in Figures 2 and 3 should be an imprint of localized stress developed within the polymer film during SRG formation. In addition, features like the convenient adaptability of the metal film on the deforming polymer surface implies the existence of a strong bonding layer at the metal/polymer interface.

To address this question, we performed neutron reflectivity measurements on plain Au/PAZO/glass sample (without grating) as described in the following section.

3.3. Analysis of the Metal/Polymer Interface Using Neutron Reflectivity. To understand the Au/PAZO interface, we performed neutron reflectivty measurements on 10 nm thin metal films deposited on a micrometer thick PAZO film spin-coated on glass substrate (further experimental details are provided in the methods section). For the modeling of neutron reflectivity curves from the given set of parameters, we used the so-called matrix formalism described in detail elsewhere.[39,40]

The boundary conditions at every interface allow one to obtain the system of linear equations in matrix form, which connects the Fresnel coefficients above the sample surface with the coefficients in the substrate. Generally, due to random roughness, the interface between two neighboring layers is described as a random Gaussian variable $z(x, y)$ with standard deviation σ. The description works correctly only in the case when $\sigma \ll t$, where t is a layer thickness. When σ is too large, one considers graded but smooth interfaces, where the scattering length density is a function of z. The interface is divided into thin slabs with a maximum thickness $t_s < 2\pi/Q_{max}$, where Q_{max} is a maximum scattering vector in the experimental data.

In order to simplify the analysis of the experimental data, we performed neutron reflectivity measurements on a pure glass substrate, PAZO/glass sample, and Au/PAZO/glass. We present in particular the modeling procedure applied to the data from all three samples and the obtained parameter.

Pure Glass. The experimental reflectivity curve and fitting result for the pure glass substrate are shown in Supporting Information (Figure S3). Fitting of experimental data led to the following optimized values of glass SLD and roughness, respectively: $(3.565 \times 10^{-6}) \pm (0.001 \times 10^{-6})$ Å^{-2} and $\sigma = 8.00 \pm 0.02$ Å.

PAZO/Glass. Simulations of the data from the PAZO/glass sample (Supporting Information, Figure S4) has shown that the profile of the rough air−polymer interface tends effectively to a form of square root gradient with the following parameters: scattering length density of PAZO film at $z = 0$ ρ_{PAZO} $(z = 0) =$

$(1.135 \times 10^{-6}) \pm (0.005 \times 10^{-6})$ Å^{-2}, gradient thickness 125.94 ± 0.50 Å, and mean SLD of PAZO = $(2.246 \times 10^{-6}) \pm (0.003 \times 10^{-6})$ Å^{-2}. The scattering length density of glass substrate and its roughness were taken from a previous fit of the data for pure glass sample.

Au/PAZO/Glass. The model of PAZO in the above section shows that the surface of the polymer is not perfect and its profile tends to a square root gradient. The AFM surface roughness analysis of 5 × 5 μm^2 demonstrates a much smaller surface roughness of around 1 nm. However, a neutron beam at low angles covers a larger surface given by the opening of the beam and gives more averaged information compared to AFM.

To simulate a profile of a gold layer and gold/PAZO interface, we used the following procedure. The first 200 Å of the scattering length density profile including the Au layer and the interface between the gold layer and PAZO film were split into 10 slices. The parameters of every slice were optimized independently with physical constrains for the slice thickness and SLD; the former could possess the values in the range from 0 to 25 Å, defined by the maximum experimental scattering vector Q_{max}, and the latter was limited from the upper side by 5×10^{-6} Å^{-2}, which is larger than the calculated value of the scattering length density of gold, 4.5×10^{-6} Å^{-2}. The result in Figure 4b shows perfect agreement between the curves. The final density profile is presented in the inset of Figure 4b.

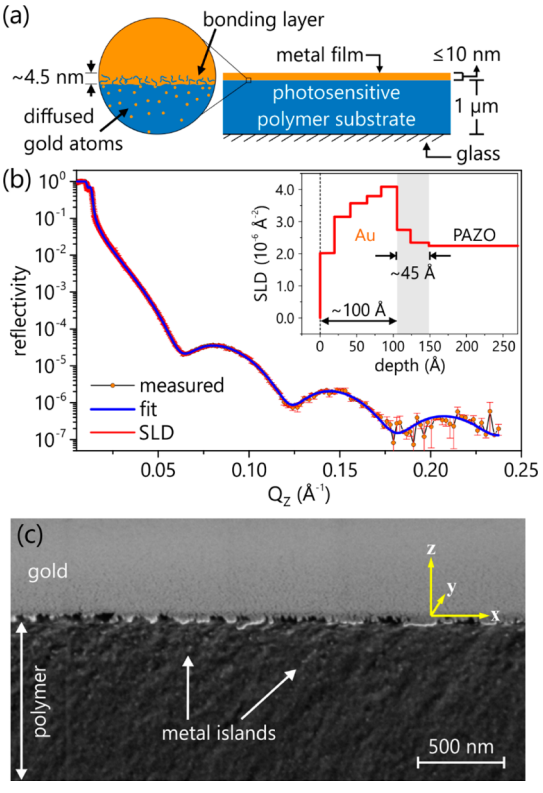

Figure 4. Neutron reflectivity analysis of the bonding layer at the metal/polymer interface. (a) Scheme of bonding layer. (b) The final scattering length density profile (embedded image) and fit results of the corresponding calculated neutron reflectivity curve. SLD and thickness of the sublayers were optimized by the Levenberg–Marquardt algorithm. (c) SEM image depicting the metal polymer interface (cross-sectional view of air/Au/polymer). The *xy*-plane indicates the gold film topography, and the *z*-axis indicates the normal to the sample surface.

The scheme in Figure 4a shows the gold/polymer/glass interface and the estimated diffused layer to be ~45 Å. In addition to neutron reflectivity, we performed SEM imaging of bisected Au/PAZO/glass sample (breaking pressure applied toward the gold layer to avoid particles from the gold layer being distributed within the polymer). The SEM image in Figure 4c shows a few single metal grains diffused deep into the polymer film. Metal particles are observed up to 500 nm deep in the polymer film; however, these small grains of metal particles are invisible for detection using neutron reflectivity due to the lack of significant particle density.

3.4. Effect of Metal/Polymer Interface on Crack Formation. The neutron reflectivity results presented in the above section clearly indicate ~45 Å thin diffused Au layer into the PAZO surface, resulting in a good bonding/adhesion layer at Au/PAZO interface. To investigate how this bonding layer influences the crack formation within the metal layer, we performed experiments in which the metal and polymer are separated by a nanoscopic thin graphene layer.

Highly oriented pyrolytic graphene (HOPG) layers from the graphite substrate are transferred onto 1 μm thick photosensitive polymer film surface using the method of mechanical exfoliation. During this procedure, pieces of multilayered graphene (G-ML) of arbitrary shape, size, and thickness are transferred on the polymer surface. Afterward, the metal layer of 10 nm in thickness is deposited on top (scheme in Figure 5a). The morphologies of the gold layer on the G-ML and the polymer surface differ significantly, allowing us to track exactly the position of the G-ML piece (Figure 5c). The average thickness of the graphite pieces spread across the polymer surface in a definite area before gold deposition was analyzed using AFM and found to be around 10 nm, indicating the multilayer structure of the graphene. From the literature it is known that there is no penetration of the gold through the graphene multilayer,[41,42] so we can be sure that on the places covered by G-ML there is no metal/polymer bonding interface. The SEM analysis after grating inscription in Au/G-ML/polymer sample is presented in Figure 5d. From the AFM cross-sectional profile (scheme in Figure 5b), one can see that the G-ML layer is centered at the topography minima and bends together with the underlying polymer surface. The presence of the G-ML piece of a width smaller than the SRG period does not alter the height of the grating topography. However, the Au layer on G-ML remains undisturbed and cracks appear only in the regions where the gold layer is in the direct contact with PAZO. This observation clearly supports the fact that the bonding layer at Au/PAZO interface serves as a transducer of the local stress distribution in the polymer film to a metal layer.

On the macroscopic level, during irradiation with an interference pattern the glassy photosensitive polymer film deforms strongly without significant photoinduced softening.[43] This implies that the stresses generated within the films during irradiation should be quite strong, at least larger than the yield point of the polymers.[29,30] Moreover, with the additional mechanical constrain in the form of the metal layer adsorbed on top, the deformation of the metal/polymer system still takes place under irradiation, indicating that the opto-mechanical stresses are even larger and can do quite an amount of work. During material mass transport the polymer film exerts forces on the metal layer adsorbed on top. The bonding interface between the polymer and metal layer serves as a transducer of the applied opto-mechanical forces. Utilizing a standard model

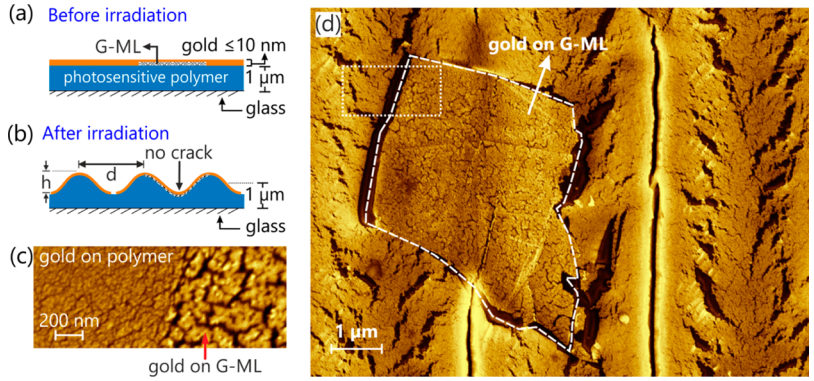

Figure 5. Schemes of Au/G-ML/polymer interface before (a) and after irradiation (b). (c) SEM micrograph of 10 nm thin gold layer deposited on polymer and G-ML surface. The micrograph is recorded on the area marked by a dotted white line in part d, where the SEM image of gold film topography deposited on a region covered with G-ML and on a polymer surface after SRG inscription is depicted. The piece of graphene is marked by the dashed white line.

frequently used for metal laminated polymer substrates that are put under tensile strain, one can estimate the stresses that the polymer exerts on the metal film.[44] From a standard equation ($\sigma = K\varepsilon^N$), we may estimate local stress to be $\sigma = 0.11$ GPa. Here we use values for the strain, $\varepsilon = 0.105$, calculated as described above; for the prefactor, $K = 114$ MPa, and the hardening exponent, $N = 0.02$, which are typical for a weakly hardening metal.[45] The continuous cracks observed in the metal layer at grating slopes and near maxima (Figure 2d,f) are difficult to decipher due to the combination of complicated mass transport and molecular reorientation processes in photosensitive material as well as bending and bulging phenomena in metal film during SRG formation.

On the molecular level the radiation field acts only on the azobenzene molecules that orient themselves perpendicularly with their main molecular axis to the direction of $\vec{E}$ field vector during multiple trans- to cis-photoisomerizations.[10,46] An external, spatially varying radiation field given by an interference pattern introduces gradients in local ordering of the azobenzenes and/or chemical potential.[11,12,47] Since the azobenzenes are tied to the polymer chains, the reorientation of azobenzene molecules perpendicularly to the polarization of light causes the reorientation of polymer backbones and, thus, the macroscopic deformation of a sample due to the strong mechanical coupling between the two phases: azobenzenes and polymer matrix. Depending on the $\vec{E}$ field vector distribution within the interference pattern, one might expect a different magnitude and local direction of the opto-mechanical stresses. Indeed, when inscribed with a different polarization pattern, the kinetics of the SRG formation changes significantly,[2] as well as the maximally attainable height of the gratings. But even when the height, periodicity, and the kinetics of the polymer film deformation are the same for two types of interference patterns, there is still significant local difference. In this study, we show that when the metal/polymer sample is irradiated with two different interference patterns (±45° and RCP:LCP), the morphology of the metal damage, i.e., shape and direction of the cracks within the metal, differs significantly. Since the gold layers are tightly bound to an upper layer of the polymer film and even partially penetrate inside, the considerable relocation of gold material along with the mass transport within the polymer implies that on a local, nanoscopic scale the distribution of the opto-mechanical stress is not uniform. In future studies small gold nanoparticles immersed within the film could be used as local probes for forces and polymer flow, thus probing transport properties with high spatial resolution.

4. CONCLUSION

In conclusion, we report on ultrathin metallized photosensitive polymer films and their response to irradiation with an interference pattern. Using neutron reflectivity, a 45 Å thick diffused metal layer into the polymer surface was found to form the bonding layer between the polymer and metal layers. The bonding or adhesion layer at the interface serves as transducer for opto-mechanical stresses that polymer material exerts on the metal layer during surface relief grating formation. The forces developed in the polymer layer under irradiation are quite strong and result in not only significant deformation in the glassy polymer material but also in a deformation and rupturing of the metal layer. When separated by the graphene multilayer, the metal film still deforms due to the increase in the surface area, but no rupturing appears within the layer. We state here that the periodic metallic cracks observed along grating are the direct imprint of opto-mechanical stress developed in the skin of the polymer layer during SRG formation. Moreover, we have shown that the distribution of the electrical field vector within the interference pattern significantly changes the local distribution of the opto-mechanical stress, even when the kinetics and value of the surface area change are kept constant. To our knowledge, this is the first reported experimental observation of a local probe of the opto-mechanical stress distribution within photosensitive polymer films.

■ ASSOCIATED CONTENT

Supporting Information

Ex-situ SEM analysis of crack formation with characteristic strain features, SEM images of periodically ruptured gold films on polymer during SRG formation, the Levenberg−Marquardt fit of a calculated neutron reflectivity curve of a glass substrate, and a calculated neutron reflectivity curve of a PAZO−air interface (Figures S1−S4). This material is available free of charge via the Internet at http://pubs.acs.org.

■ AUTHOR INFORMATION

Corresponding Author

*E-mail: sekhar@uni-potsdam.de or ynatarajasekhar@hotmail.com.

Notes

The authors declare no competing financial interest.

■ ACKNOWLEDGMENTS

The work is supported by the priority program SPP-1369 (DFG) and Volkswagen Stiftung, Germany. We would like to thank Dr. Alexey Kopyshev for valuable discussions and graphic work. We would like to acknowledge Prof. Dr. Sc. Oleg Vyvenko and Dr. Yuri Petrov from the Interdisciplinary Resource Center for Nanotechnology (St. Petersburg, Russia) for their valuable support in the use of the Zeiss Supra 40VP scanning electron microscope.

■ REFERENCES

(1) Rau, H. Photoisomerization of azobenzenes. In *Photochemistry and Photophysics*; Rabeck, J. F., Ed.; CRC Press: Boca Raton, FL, 1990; Vol *III*, pp 119−141.

(2) Yadavalli, N. S.; Santer, S. In-situ Atomic Force Microscopy Study of the Mechanism of Surface Relief Grating Formation in Photosensitive Polymer Films. *J. Appl. Phys.* **2013**, *113*, 224304.

(3) Yadavalli, N. S.; Saphiannikova, S.; Lomadze, N.; Goldenberg, L. M.; Santer, S. Structuring of Photosensitive Material below Diffraction Limit Using Far Field Irradiation. *Appl. Phys. A: Mater. Sci. Process.* **2013**, *113*, 263−272.

(4) Cembran, A.; Bernardi, F.; Garavelli, M.; Gagliardi, L.; Orlandi, G. On the Mechanism of the Cis−Trans Isomerization in the Lowest Electronic States of Azobenzene: S_0, S_1, and T_1. *J. Am. Chem. Soc.* **2004**, *126*, 3234−3243.

(5) Rochon, P.; Batalla, E.; Natansohn, A. Optically Induced Surface Gratings on Azoaromatic Polymer Films. *Appl. Phys. Lett.* **1995**, *66*, 136−138.

(6) Kim, D. Y.; Tripathy, S. K.; Li, L.; Kumar, J. Laser-Induced Holographic Surface Relief Gratings on Nonlinear Optical Polymer Films. *Appl. Phys. Lett.* **1995**, *66*, 1166−1168.

(7) Yadavalli, N. S.; Saphiannikova, M.; Santer. S. Photosensitive Response of Azobenzene Containing Films towards Pure Intensity or Polarization Interference Patterns. *Appl. Phys. Lett.* **2014**, in press (access date: 1st Aug, 2014, cover page featured article).

(8) Kulikovska, O.; Gharagozloo-Hubmann; Stumpe, J. Polymer Surface Relief Structures caused by Light-Driven Diffusion. *Proc. SPIE* **2002**, *4802*, 85−92.

(9) Barrett, C.; Natansohn, A.; Rochon, P. Cis−Trans Thermal Isomerization Rates of Bound and Doped Azobenzenes in a Series of Polymers. *Chem. Mater.* **1995**, *7*, 899−903.

(10) Seki, T.; Fukuda, K.; Ichimura, K. Photocontrol of Polymer Chain Organization using a Photochromic Monolayer. *Langmuir* **1999**, *15*, 5098−5101.

(11) Ambrosio, A.; Marrucci, L.; Borbone, F.; Roviello, A.; Maddalena, P. Light-Induced Spiral Mass Transport in Azo-Polymer Films under Vortex-Beam Illumination. *Nat. Commun.* **2012**, *3*, 989.

(12) Nikolova, L.; Ramanujam, P. S. *Polarization Holography*; Cambridge Academic Press: UK, 2009; pp 88−140.

(13) Natansohn, A.; Rochon, P.; Ho, M. S.; Barrett, C. Azo Polymers for Reversible Optical Storage. 6. Poly[4-[2-(methacryloyloxy)ethyl]-azobenzene. *Macromolecules* **1995**, *28*, 4179−4183.

(14) Yi, D. K.; Seo, E. M.; Kim, D. Y. Surface-Modulation-Controlled Three-Dimensional Colloidal Crystals. *Appl. Phys. Lett.* **2002**, *80*, 225−227.

(15) Divliansky, I. B.; Shishido, A.; Khoo, I.; Mayar, T. S.; Pena, D.; Nishimura, S.; Keating, C. D.; Mallouk, T. E. Fabrication of Two-Dimensional Photonic Crystals using Interference Lithography and Electrodeposition of CdSe. *Appl. Phys. lett.* **2001**, *79*, 3392−3394.

(16) Sreekanth, K. V.; Chua, J. K.; Murukeshan, V. M. Interferometric Lithography for Nanoscale Feature Patterning: A Comparative Analysis between Laser Interference, Evanescent Wave Interference, and Surface Plasmon Interference. *Appl. Opt.* **2010**, *49*, 6710−6717.

(17) Na, S.; Kim, S.; Jo, J.; Oh, S.; Kim, J.; Kim, D. Efficient Polymer Solar Cells with Surface Relief Gratings Fabricated by Simple Soft Lithography. *Adv. Funct. Mater.* **2008**, *18*, 3956−3963.

(18) Lee, S.; Kang, H. S.; Park, J. Directional Photofluidization Lithography: Micro/Nanostructural Evolution by Photofluidic Motions of Azobenzene Materials. *Adv. Mater.* **2012**, *24*, 2069−2103.

(19) Lagugne Labarthet, F.; Bruneel, J. L.; Buffeteau, T.; Sourisseau, C. Chromophore Orientations upon Irradiation in Gratings Inscribed on Azo-Dye Polymer Films: A Combined AFM and Confocal Raman Microscopic Study. *J. Phys. Chem. B* **2004**, *108*, 6949−6960.

(20) Lagugne Labarthet, F.; Sourisseau, C.; Schaller, R. D.; Saykally, R. J.; Rochon, P. Chromophore Orientations in a Nonlinear Optical Azopolymer Diffraction Grating: Even and Odd Order Parameters from Far-Field Raman and Near-Field Second Harmonic Generation Microscopies. *J. Phys. Chem. B* **2004**, *108*, 17059−17068.

(21) Lagugne Labarthet, F.; Bruneel, J. L.; Rodriguez, V.; Sourisseau, C. Chromophore Orientations in Surface Relief Gratings with Second-Order Nonlinearity As Studied by confocal Polarized Raman Microspectrometry. *J. Phys. Chem. B* **2004**, *108*, 1267−1278.

(22) Di Florio, G.; Brüdermann; Yadavalli, N. S.; Santer, S.; Havenith, M. Polarized 3D Raman and Nanoscale Near-Field Field Optical Microscopy of Optically Inscribed Surface Relief Gratings: Chromophore Orientation in Azo-Doped Polymer Films. *Soft Matter* **2014**, *10*, 1544−1554.

(23) Bian, S.; Li, L.; Kumar, J.; Kim, D. Y.; Williams, J.; S. Tripathy, K. Single Laser Beam-Induced Surface Deformation on Azobenzene Polymer Films. *Appl. Phys. Lett.* **1998**, *73*, 1817.

(24) Kumar, J.; Li, L.; Xiang, X. L.; Kim, D. Y.; Lee, T. S.; Tripathy, S. Gradient Force: The Mechanism for Surface Relief Grating Formation in Azobenzene Functionalized Polymers. *Appl. Phys. Lett.* **1998**, *72*, 2096.

(25) Jiang, X. L.; Li, L.; Kumar, J.; Kim, D. Y.; Tripathy, S. K. Unusual Polarization Dependent Optical Erasure of Surface Relief Gratings on Azobenzene Polymer Films. *Appl. Phys. Lett.* **1998**, *72*, 2502.

(26) Pedersen, T. G.; Johansen, P. M.; Holme, N. C. R.; Ramanujam, P. S.; Hvilsted, S. Mean-Field Theory of Photoinduced Formulation of Surface Reliefs in Side-Chain Azobenzene Polymers. *Phys. Rev. Lett.* **1998**, *80*, 89−92.

(27) Bublitz, D.; Fleck, B.; Wenke, L. A Model for Surface-Relief Formation in Azobenzene Polymers. *Appl. Phys. B: Laser Opt.* **2001**, *72*, 931.

(28) Saphiannikova, M.; Neher, D. Thermodynamic Theory of Light-Induced Material Transport in Amorphous Azobenzene Polymer Films. *J. Phys. Chem. B* **2005**, *109*, 19428.

(29) Toshchevikov, V.; Saphiannikova, M.; Heinrich, G. Microscopic Theory of Light-Induced Deformation in Amorphous Side-Chain Azobenzene Polymers. *J. Phys. Chem. B* **2009**, *113*, 5032.

(30) Toshchevikov, V.; Saphiannikova, M.; Heinrich, G. Light-Induced Deformation of Azobenzene Elastomers: A Regular Cubic Network Model. *J. Phys. Chem. B* **2012**, *116*, 913.

(31) Geue, T. M.; Saphiannikova, M. G.; Henneberg, O.; Pietsch, U. Formation Mechanism and Dynamics in Polymer Surface Gratings. *Phys. Rev. E* **2002**, *65*, 052801.

(32) Barada, D.; Itoh, M.; Yatagai, T. Computer Simulations of Photoinduced Mass Transport on Azobenzene Polymer Films by Particle Method. *J. Appl. Phys.* **2004**, *96*, 4204.

(33) Saphiannikova, M.; Geue, T. M.; Henneberg, O.; Morawetz, K.; Pietsch, U. Linear Viscoelastic Analysis of Formation and Relaxation of Azobenzene Polymer Gratings. *J. Chem. Phys.* **2004**, *120*, 4039.

(34) Yadavalli, N. S.; Linde, F.; Kopyshev, A.; Santer, S. Soft Matter Beats Hard Matter: Rupturing of Thin Metallic Films Induced by Mass Transport in Photosensitive Polymer Films. *ACS Appl. Mater. Interfaces* **2013**, *5*, 7743−7747.

(35) Leosson, K.; Ingason, A. S.; Agnarsson, B.; Kossoy, A.; Olafsson, S.; Gather, M. C. Ultra-Thin Gold Films on Transparent Polymers. *Nanophotonics* **2013**, *2*, 3−11.

(36) Linde, F.; Yadavalli, N. S.; Santer, S. Conductivity Behavior of Very Thin Gold Films Ruptured by Mass Transport in Photosensitive Polymer Film. *Appl. Phys. Lett.* **2013**, *103*, 253101.
(37) Lu, N.; Wang, X.; Suo, Z.; Vlassak, J. Failure by Simultaneous Grain Growth, Strain Localization, and Interface Debonding in Metal Films on Polymer Substrates. *J. Mater. Res.* **2008**, *24*, 379−385.
(38) Tellez, H.; Vadillo, J. M.; Laserna, J. J. Energy-Resolved Depth Profiling of Metal−Polymer Interfaces Using Dynamic Quadrupole Secondary Ion Mass Spectrometry. *Rapid Commun. Mass Spectrom.* **2009**, *23*, 2357−2362.
(39) Stepanov, S. A.; Kondrashkina, E. A.; Koehler, R.; Novikov, D. V.; Materlik, G.; Durbin, S. M. Dynamical X-Ray Diffraction of Multilayers and Superlattices: Recursion Matrix Extension to Grazing Angles. *Phys. Rev. B* **1998**, *57*, 4829−4841.
(40) Abeles, F. F. Recherches sur la Propagation des Ondes Electromagnetiques Sinusoidales dans les Milieus Stratifies. *Ann. Phys. (Paris)* **1950**, *5*, 596−640.
(41) Zan, R.; Bangert, U.; Ramasse, Q.; Novoseloc, K. S. Evolution of Gold Nanostructures on Graphene. *Small* **2011**, *7*, 2868−2872.
(42) Liu, X.; Wang, C.-Z.; Hupalo, M.; Lin, H.-Q.; Ho, K.-M.; Tringides, M. C. Metals on Graphene: Interactions, Growth Morphology, and Thermal Stability. *Crystals* **2013**, *3*, 79−111.
(43) Saphiannikova, M.; Toshchevikov, V.; Ilnytskyi, J. Photoinduced Deformations in Azobenzene Polymer Films. *Nonlinear Opt., Quantum Opt.* **2010**, *41*, 27−57.
(44) Li, T.; Huang, Z. Y.; Xi, Z. C.; Lacour, S. P.; Wagner, S.; Suo, Z. Delocalizing Strain in a Thin Metal Film on a Polymer Substrate. *Mech. Mater.* **2005**, *37*, 261−273.
(45) Li, T.; Suo, Z. Deformability of Thin Metal Films on Elastomer Substrates. *Int. J. Solids Struct.* **2006**, *43*, 2351−2363.
(46) Barrett, C.; Natansohn, A.; Rochon, P. Cis−Trans Thermal Isomerization Rates of Bound and Doped Azobenzenes in a Series of Polymers. *Chem. Mater.* **1995**, *7*, 899−903.
(47) Viswanathan, N. K.; Balasubramanian, S.; Li, L.; Tripathy, S. K.; Kumar, J. A Detailed Investigation of the Polarization-Dependent Surface-Relief-Grating Formation Process on Azo Polymer Films. *Jpn. J. Appl. Phys.* **1999**, *38*, 5928−5937.